1.5-T DT fiber tractography, both performed with parallel imaging, were compared in a relatively large number of subjects. Improved image quality was observed at 3.0-T tractography of the corticospinal tract.

More complex results were observed at tractography of the superior longitudinal fasciculus. Although the right superior longitudinal fasciculus was visualized significantly better at 3.0 T, the depiction score for left superior longitudinal fasciculus tractography did not differ significantly between 3.0 and 1.5 T. The numbers of tract fibers depicted at 3.0 T were significantly higher than the numbers of fibers depicted at 1.0 T. We speculated that the reason for this was as follows: According to fiber dissection study findings, the corticospinal tract is a long projection fiber bundle with a well-established anatomic distribution (35). Most fibers in the corticospinal tract run parallel through the posterior limb of the internal capsule, without sharp turning angles or directional diversity.

Conversely, both the superior longitudinal fasciculus and the corpus callosum consist of groups of fiber bundles that comprise association or commissural fibers of varying lengths and directions. The superior longitudinal fasciculus contains arcuate fibers that turn sharply toward the temporal lobe. This sharp turning angle may surpass the tracking terminate threshold, and tracking does not extend to reach the temporal lobe. Temporal fibers are susceptible to image distortion at the middle cranial fossa and temporal bone, where the air-tissue interface induces magnet susceptibility artifacts. Thus, we propose that temporal arcuate fibers are more affected by image distortion than are long association fibers. In the present study, left arcuate fibers were visualized in a larger number of subjects than were right arcuate fibers at both 3.0 and 1.5 T. Such asymmetry of the arcuate fibers at tractography may be due to image distortion or the known lateral asymmetry of temporal fibers (36), and, thus, differences between 3.0- and 1.5-T DT imaging may be underestimated on the left side.

Table 2

Analyses of Tract Depiction Scores and Numbers of Tract Fibers

Tract	Difference in Depiction Score*	*P* Value†	Difference in No. of Tract Fibers*	*P* Value‡
Right corticospinal tract§	0.87 ± 0.15	<.001	27 ± 12	.008
Left corticospinal tract	1.32 ± 0.21	<.001	70 ± 9.2	<.001
Right superior longitudinal fasciculus	0.52 ± 0.16	.005	192 ± 57	.001
Left superior longitudinal fasciculus	0.03 ± 0.14	NS	65 ± 34	.02
Corpus callosum	0.34 ± 0.12	.01	220 ± 149	NS
Right fornix	0.35 ± 0.16	.04	...	...
Left fornix	0.19 ± 0.15	NS	...	...
Left and right fornices	...	...	14 ± 5.5	.02

Note.—NS = not significant.

* Data are mean difference values ± standard deviations.

† *P* values for difference in depiction scores at 1.5- versus 3.0-T tractography.

‡ *P* values for difference in numbers of tract fibers at 1.5- versus 3.0-T tractography.

§ The mean asymmetry index for the corticospinal tract was 0.47 ± 0.11 (standard deviation), and the difference in corticospinal tract asymmetry index at 1.5- versus 3.0-T tractography was significant ($P < .001$).

For corpus callosum tractography, tract depiction scores were better at 3.0 T than at 1.5 T but the numbers of tract fibers did not differ significantly. At corpus callosum tractography, the crossing-fiber problem of unidirectional tracking models (37) may contribute to the discrepancies observed between depiction scores and tract fiber numbers. Corpus callosum tractography is susceptible to the crossing-fiber problem at the centrum semiovale. In this area, a small number of callosal fibers intersect a large number of corticospinal tract fibers. Thus, corpus callosum tractography might reveal a smaller number of fibers than the appropriate fiber trajectory owing to limitations related to the crossing-fiber problem, and differences between 3.0- and 1.5-T imaging may be underestimated.

The statistical methods used may have been responsible for the differences in results obtained at analyses of the depiction scores and the numbers of tract fibers. Although mean differences in the numbers of depicted fibers between 3.0- and 1.5-T imaging were as large as 220, no significant difference was noted. This was probably because of the relatively large numbers of depicted fibers (mean numbers: 3784 at 3.0 T and 3565 at 1.5 T). Low statistical power also may have contributed to this lack of a significant difference.

Depiction scores for right fornix tractography were significantly better at 3.0 T than at 1.5 T, but no significant differences were noted for the left fornix. The numbers of tract fibers depicted at 3.0-T fornix tractography were significantly higher than the numbers depicted at 1.5-T tractography. This result was probably due to the relatively lower volume of limbic fibers compared with the volumes of other fiber bundles. Our DT imaging voxel size was 1.7 × 1.7 × 3.0 mm. The body and crus of the fornix are composed of narrow fiber bundles—they are smaller in diameter than a single voxel—so partial volume-averaging artifacts would have had a greater effect in this region than in the other fiber tracts.

The present study had some limitations. First, the imaging parameters for 3.0-T imaging were not optimized to achieve the best DT image quality. For the most part, we used identical imaging parameters to perform 3.0- and 1.5-T imaging for comparisons so that features other than magnetic field strength would be equivalent. However, differences in T1 and T2* interfere with the equal conditions between 3.0- and 1.5-T imaging. A DT imaging sequence optimized for 1.5-T imaging is not the optimal sequence for 3.0-T imaging. The differences in bandwidth between 3.0- and 1.5-T imaging also may have biased

our results. We tried to keep other acquisition parameters equivalent between 3.0- and 1.5-T imaging, but the bandwidth was higher at 3.0 T. Higher bandwidth results in a reduced signal-to-noise ratio and reduced image distortion. DT imaging at 3.0 T yields a higher signal-to-noise ratio and causes greater magnet susceptibility artifacts owing to the higher static magnetic field strength. We adjusted parameters so that we could use a bandwidth of 1502 Hz per pixel for 3.0-T imaging, which is up to 50% higher than the bandwidth used for 1.5-T imaging. Further optimization of 3.0-T imaging to improve the quality of DT images may be required in the future.

Second, the development of imaging methods to reduce the effects of the crossing-fiber problem, such as high angular DT imaging with high *b* values (38) and diffusion-spectrum imaging (36), is progressing. Other fiber-tracking methods, such as probabilistic tractography to estimate the probability of fiber connections through the data field (39), also are advancing. These advanced methods will affect the results of both 3.0-T and 1.5-T tractography.

In conclusion, DT tractography at 3.0 T enables improved visualization of the corticospinal tract compared with DT tractography at 1.5 T, and 3.0-T tractography of the superior longitudinal fasciculus, corpus callosum, and fornix has some advantages over 1.5-T tractography. Advances in efficient MR sequences are needed to improve the image quality and reliability of 3.0-T DT tractography.

References

1. Basser PJ, Mattiello J, LeBihan D. MR diffusion tensor spectroscopy and imaging. Biophys J 1994;66:259–267.
2. Beaulieu C. The basis of anisotropic water diffusion in the nervous system: a technical review. NMR Biomed 2002;15:435–455.
3. Chenevert TL, Brunberg JA, Pipe JG. Anisotropic diffusion in human white matter: demonstration with MR techniques in vivo. Radiology 1990;177:401–405.
4. Pierpaoli C, Jezzard P, Basser PJ, Barnett A, Di Chiro G. Diffusion tensor MR imaging of the human brain. Radiology 1996;201:637–648.
5. Basser PJ, Pajevic S, Pierpaoli C, Duda J, Aldroubi A. In vivo fiber tractography using DT-MRI data. Magn Reson Med 2000;44:625–632.
6. Mori S, van Zijl PC. Fiber tracking: principles and strategies—a technical review. NMR Biomed 2002;15:468–480.
7. Masutani Y, Aoki S, Abe O, Hayashi N, Otomo K. MR diffusion tensor imaging: recent advance and new techniques for diffusion tensor visualization. Eur J Radiol 2003;46:53–66.
8. Dong Q, Welsh RC, Chenevert TL, et al. Clinical applications of diffusion tensor imaging. J Magn Reson Imaging 2004;19:6–18.
9. Stieltjes B, Kaufmann WE, van Zijl PC, et al. Diffusion tensor imaging and axonal tracking in the human brainstem. Neuroimage 2001;14:723–735.
10. Wakana S, Jiang H, Nagae-Poetscher LM, van Zijl PC, Mori S. Fiber tract–based atlas of human white matter anatomy. Radiology 2004;230:77–87.
11. Clark CA, Barrick TR, Murphy MM, Bell BA. White matter fiber tracking in patients with space-occupying lesions of the brain: a new technique for neurosurgical planning? Neuroimage 2003;20:1601–1608.
12. Yamada K, Kizu O, Mori S, et al. Brain fiber tracking with clinically feasible diffusion-tensor MR imaging: initial experience. Radiology 2003;227:295–301.
13. Huisman TA, Schwamm LH, Schaefer PW, et al. Diffusion tensor imaging as potential biomarker of white matter injury in diffuse axonal injury. AJNR Am J Neuroradiol 2004;25:370–376.
14. Glenn OA, Henry RG, Berman JI, et al. DTI-based three-dimensional tractography detects differences in the pyramidal tracts of infants and children with congenital hemiparesis. J Magn Reson Imaging 2003;18:641–648.
15. Kunimatsu A, Aoki S, Masutani Y, Abe O, Mori H, Ohtomo K. Three-dimensional white matter tractography by diffusion tensor imaging in ischaemic stroke involving the corticospinal tract. Neuroradiology 2003;45:532–535.
16. Tanenbaum LN. 3-T MR imaging: ready for clinical practice [letter]. AJNR Am J Neuroradiol 2004;25:1626–1627.
17. Zhai G, Lin W, Wilber KP, Gerig G, Gilmore JH. Comparisons of regional white matter diffusion in healthy neonates and adults performed with a 3.0-T head-only MR imaging unit. Radiology 2003;229:673–681.
18. Sodickson DK, Manning WJ. Simultaneous acquisition of spatial harmonics (SMASH): fast imaging with radiofrequency coil arrays. Magn Reson Med 1997;38:591–603.
19. Pruessmann KP, Weiger M, Scheidegger MB, Boesiger P. SENSE: sensitivity encoding for fast MRI. Magn Reson Med 1999;42:952–962.
20. Griswold MA, Jakob PM, Heidemann RM, et al. Generalized autocalibrating partially parallel acquisitions (GRAPPA). Magn Reson Med 2002;47:1202–1210.
21. van den Brink JS, Watanabe Y, Kuhl CK, et al. Implications of SENSE MR in routine clinical practice. Eur J Radiol 2003;46:3–27.
22. Jaermann T, Crelier G, Pruessmann KP, et al. SENSE-DTI at 3 T. Magn Reson Med 2004;51:230–236.
23. Naganawa S, Koshikawa T, Kawai H, et al. Optimization of diffusion-tensor MR imaging data acquisition parameters for brain fiber tracking using parallel imaging at 3 T. Eur Radiol 2004;14:234–238.
24. Nagae-Poetscher LM, Jiang H, Wakana S, Golay X, van Zijl PC, Mori S. High-resolution diffusion tensor imaging of the brain stem at 3 T. AJNR Am J Neuroradiol 2004;25:1325–1330.
25. Bastin ME, Armitage PA. On the use of water phantom images to calibrate and correct eddy current induced artefacts in MR diffusion tensor imaging. Magn Reson Imaging 2000;18:681–687.
26. Pajevic S, Pierpaoli C. Color schemes to represent the orientation of anisotropic tissues from diffusion tensor data: application to white matter fiber tract mapping in the human brain. Magn Reson Med 1999;42:526–540.
27. Naidich TP, Valavanis AG, Kubik S. Anatomic relationships along the low-middle convexity. I. Normal specimens and magnetic resonance imaging. Neurosurgery 1995;36:517–532.
28. Mori S, Kaufmann WE, Davatzikos C, et al. Imaging cortical association tracts in the human brain using diffusion-tensor-based axonal tracking. Magn Reson Med 2002;47:215–223.
29. Lazar M, Field AS, Lee J, et al. Lateral asymmetry of superior longitudinal fasciculus: a white matter tractography study (abstr). In: Proceedings of the 12th Meeting of the International Society for Magnetic Resonance in Medicine. Berkeley, Calif: International Society for Magnetic Resonance in Medicine, 2004; 1290.

30. Fera F, Yongbi MN, van Gelderen P, Frank JA, Mattay VS, Duyn JH. EPI-BOLD fMRI of human motor cortex at 1.5 T and 3.0 T: sensitivity dependence on echo time and acquisition bandwidth. J Magn Reson Imaging 2004;19:19–26.

31. Willinek WA, Born M, Simon B, et al. Time-of-flight MR angiography: comparison of 3.0-T imaging and 1.5-T imaging—initial experience. Radiology 2003;229:913–920.

32. Willinek WA GJ, von Falkenhausen M, et al. 3.0T contrast-enhanced, submillimeter MRA of the supraaortic arteries: does the signal gain at high field strength allow to replace the phased array coil by the quadrature body coil? (abstr). In: Proceedings of the 12th Meeting of the International Society for Magnetic Resonance in Medicine. Berkeley, Calif: International Society for Magnetic Resonance in Medicine, 2004; 1523.

33. Graf H, Schick F, Claussen CD, Seemann MD. MR visualization of the inner ear structures: comparison of 1.5 Tesla and 3 Tesla images. Rofo 2004;176:17–20.

34. Hunsche S, Moseley ME, Stoeter P, Hedehus M. Diffusion-tensor MR imaging at 1.5 and 3.0 T: initial observations. Radiology 2001; 221:550–556.

35. Yagishita A, Nakano I, Oda M, Hirano A. Location of the corticospinal tract in the internal capsule at MR imaging. Radiology 1994;191:455–460.

36. Lin CP, Wedeen VJ, Chen JH, Yao C, Tseng WY. Validation of diffusion spectrum magnetic resonance imaging with manganese-enhanced rat optic tracts and ex vivo phantoms. Neuroimage 2003;19:482–495.

37. Wiegell MR, Larsson HB, Wedeen VJ. Fiber crossing in human brain depicted with diffusion tensor MR imaging. Radiology 2000; 217:897–903.

38. Tuch DS, Reese TG, Wiegell MR, Makris N, Belliveau JW, Wedeen VJ. High angular resolution diffusion imaging reveals intravoxel white matter fiber heterogeneity. Magn Reson Med 2002;48:577–582.

39. Behrens TE, Woolrich MW, Jenkinson M, et al. Characterization and propagation of uncertainty in diffusion-weighted MR imaging. Magn Reson Med 2003;50:1077–1088.

Evaluation of Primary Brain Tumors With FLT-PET: Usefulness and Limitations

Tsuneo Saga, MD, Hidekazu Kawashima,* Norio Araki,† Jun A. Takahashi,‡ Yasuaki Nakashima,§ Tatsuya Higashi,* Natsuo Oya,‖ Takahiro Mukai,¶ Masato Hojo,‡ Nobuo Hashimoto,‡ Toshiaki Manabe,§ Masahiro Hiraoka,† and Kaori Togashi**

Purpose of the Report: The purpose of this report was to investigate the potential of positron emission tomography using F-18 fluorodeoxythymidine (FLT-PET) in evaluating primary brain tumors.

Materials and Methods: FLT-PET was performed in 25 patients with primary brain tumors. FLT uptake in the lesion was semiquantitatively evaluated by measuring the maximal standardized uptake value (SUVmax) and the tumor-to-normal tissue ratio (TNR). SUVmax and TNR were compared with the histologic grade and the expression of the proliferation marker (Ki-67).

Results: FLT uptake in normal brain parenchyma was very low, resulting in the visualization of brain tumors with high contrast. Both SUVmax and TNR significantly correlated with the malignant grade of brain gliomas, in which high SUVmax/TNR was obtained for high-grade gliomas. Patients with primary lymphoma also showed SUVmax/TNR equivalent to glioblastoma. There was a positive correlation between SUVmax/TNR and the Ki-67 index. In contrast, spuriously high SUVmax and TNR were obtained in 3 of 6 patients with suspected recurrent tumors (2 patients with recurrent grade 2 glioma and one patient with postoperative granuloma), all of which showed lesion enhancement on MRI after Gd administration.

Conclusions: FLT-PET can be used to evaluate the malignant grade and proliferation activity of primary brain tumors, especially malignant brain tumors. However, the presence of benign lesions showing blood–brain barrier disruption cannot be distinguished from malignant tumors and needs to be carefully evaluated.

Key Words: positron emission tomography, fluorothymidine, brain tumor, malignant grade, proliferation

(*Clin Nucl Med* 2006;31: 774–780)

For the evaluation of brain tumors, morphologic imaging modalities such as computed tomography (CT) and magnetic resonance imaging (MRI) have been routinely used. However, these modalities cannot fully characterize brain tumors, because they have limitations in evaluating the malignant grade, in differentiating recurrent lesion from radiation necrosis, and so on.[1,2] For these purposes, nuclear medicine procedures using radiopharmaceuticals labeled with single-photon and positron emitters have been applied.[3] Recently, positron emission tomography (PET) using F-18 fluoro-2-deoxy-D-glucose (FDG) has been widely applied for the management of patients with clinical cancer.[4] In the evaluation of brain tumors, FDG-PET, which can noninvasively visualize increased glucose metabolism in cancerous tissues, has been used not only to detect tumors, but also used for tumor grading, the evaluation of treatment response, and the differentiation of recurrent lesions from radiation necrosis.[5] However, normal gray matter also has increased glucose metabolism and FDG-PET has a limitation in evaluating tumors with low glucose metabolism.[6,7] Furthermore, FDG is known to accumulate in inflammatory tissues.[8]

Recently, F-18 deoxy-3′-fluorothymidine (FLT), a fluorinated thymidine analog, has been emerging as a promising PET tracer to evaluate tumor proliferation activity and has been applied for various malignant tumors.[9] FLT-PET, which can image tumor proliferation, seems to be suitable for the evaluation of the malignant grade of brain tumors and also for the evaluation of treatment response. In this article, we used FLT-PET for the evaluation of primary brain tumors and compared the FLT-PET results with the histologic diagnoses and immunohistochemically determined proliferation marker expression.

PATIENTS AND METHODS

Patients

Twenty-five consecutive patients (12 men and 13 women; age range, 9–87 years; mean age, 49 years) with suspected

Received for publication January 31, 2006; revision accepted August 18, 2006.

From the Departments of *Diagnostic Imaging and Nuclear Medicine, †Therapeutic Radiology and Oncology, ‡Neurosurgery, and §Clinical Pathology, Graduate School of Medicine, Kyoto University, Kyoto, Japan; the ‖Department of Radiation Oncology, Faculty of Medical and Pharmaceutical Sciences, Kumamoto University; and the ¶Department of Chemo-Pharmaceutical Sciences, Graduate School of Pharmaceutical Sciences, Kyushu University.

Part of this investigation was supported by Grants-in-Aid for Scientific Research (15591269 and 17591265) from the Japanese Ministry of Education, Culture, Sports, Science and Technology.

Reprints: Tsuneo Saga, MD, Department of Diagnostic Imaging, Molecular Imaging Center, National Institute of Radiological Sciences, 4-9-1 Anagawa, Inage-ku, Chiba 263-8555, Japan. E-mail: saga@nirs.go.jp.

ISSN: 0363-9762/06/3112-0774

TABLE 1. Patient Data Preoperatively

Age	Sex	SUVmax	TNR	Histologic Diagnosis	Ki-67 Index
45	F	14.50	43.94	Malignant lymphoma*	100%
75	M	6.07	20.93	Glioblastoma	50%
71	F	5.43	18.72	Malignant lymphoma*	80%
66	M	3.35	12.88	Malignant lymphoma*	N/A
53	F	1.26	4.20	Glioblastoma	10%
23	M	1.03	4.12	Glioblastoma	10%
54	M	1.00	2.86	Oligodendroglioma, grade 3	50%
60	F	1.00	2.86	Astrocytoma, grade 3	10%
36	M	0.49	1.17	Astrocytoma, grade 2	7%

*All malignant lymphoma cases are diffuse large B-cell type.

primary brain tumors by MRI/CT were included in this investigation. Among 25 patients, 9 (group A) were preoperative cases without known histology, 10 (group B) were postbiopsy/partial removal cases before chemotherapy and/or radiation therapy, and the remaining 6 (group C) were suspected of tumor recurrence during the posttreatment period. Patient characteristics and FLT-PET results are summarized in Tables 1 through 3. The study plan was approved by the Institutional Ethical Committee and informed consent was obtained from all patients before FLT-PET examination.

Histopathologic diagnosis was performed based on the World Health Organization histopathologic classification. The proliferation activity of the tumor was determined by measuring the Ki-67 staining index obtained by immunohistochemical staining with anti-Ki-67/MIB-1.[10] Immunostained slides were examined at high-power magnification (×400). The percentage of positive cells was measured in the area containing the largest number of Ki-67-positive cells and was regarded as representative of the tumor proliferation activity.

TABLE 2. Patient Data: Preoperative

Age	Sex	Histologic Diagnosis	Ki-67 Index	SUVmax	TNR
87	M	Glioblastoma	40%	4.48	15.45
52	M	Glioblastoma	9%	2.52	10.96
67	F	Glioblastoma	N/A	2.44	14.35
55	F	Pineal tumor*	15%	2.11	6.59
54	M	Glioblastoma	20%	1.85	8.04
26	F	Glioblastoma	0%	1.25	4.17
26	M	Oligodendroglioma, grade 2	15%	1.06	3.93
29	F	Astrocytoma, grade 2	N/A	0.97	2.62
55	M	Astrocytoma, grade 2	1%	0.41	1.95
15	F	Ependymoma, grade 2	5%	0.31	1.48

*Pineal parenchymal tumor of intermediate differentiation.

Synthesis of FLT

FLT was radiosynthesized using a multipurpose synthesizer originally developed in our institute. F-18 fluoride in enriched target O-18 water was produced as previously described[11] and then separated from target water (4 mL) by passing the solution through a short plug of ion exchange resin. Resin-bound activity was eluted with aqueous 33 mM potassium carbonate (350 μL). The eluate was collected in a reaction glass vessel containing 50 μmol Kryptofix 222 (in 1.5 mL of acetonitrile). The reaction vessel was placed in a heating block at 140°C and then solvent was removed by azeotropic distillation with acetonitrile (3 × 1 mL) under nitrogen. Ten milligrams (19 μmol) precursor (5′-O-(4,4′-dimethoxytrityl)-2,3′-anhydrothymidine) in 1 mL of dry DMSO was added to the final residue followed by F-18 fluorination at 180°C for 10 minutes. After fluorination, the precursor was hydrolyzed by 1 N HCl (350 μL) at 65°C for 10 minutes, 1.5 mL of sodium acetate was added, and it was transferred to a reservoir containing 4 mL water. The cooled reaction mixture was loaded on to a SepPak C-18 cartridge; FLT was trapped and then washed with water (12 mL) to remove F-18 fluoride and water-soluble impurities. FLT was eluted by passing 2 mL of DMSO loaded into the injector of a semipreparative C-18 HPLC system (column: JASCO Megapak SIL C18-10 [7.5 × 250 mm], mobile phase: ethanol/water [10/90], flow rate: 5.0 mL/min). The column eluate

TABLE 3. Patient Data: Recurrence Suspected

Age	Sex	Initial Diagnosis	Treatment	Interval	SUVmax	TNR	Histologic Diagnosis	Ki-67 Index
52	F	Astrocytoma, grade 2	Operation/RT	24 mo	5.51	14.13	Glioblastoma	70%
54	F	Malignant lymphoma	CT	5 mo	4.82	11.48	Malignant lymphoma*	N/A
9	M	Ganglioglioma	Operation/RT/CT	8 mo	2.58	11.22	Ganglioglioma, grade 1	5%
54	F	Pilocytic astrocytoma	Operation	16 mo	2.09	7.21	Glioblastoma	15%
38	F	Oligodendroglioma	γ-Knife	4 mo	1.74	6.44	Astrocytoma, grade 2	1%
61	M	Glioblastoma	Operation/RT/CT	13 mo	1.65	5.89	Granuloma	0%

*Diffuse large B-cell type.
RT indicates radiation therapy; CT, chemotherapy.

was monitored by serial ultraviolet (254 nm) and gamma ray detectors and the FLT fraction eluted 9 minutes after injection was collected in a flask and evaporated to remove ethanol. The solution was then routed through a Millipore filter (0.22 μm) into a septum-sealed, sterile, pyrogen-free glass vial.

The radioactivity of the prepared FLT was 63.7 ± 37.0 MBq at EOS (yield 9.8 ± 4.3%, EOB). When the FLT solution was analyzed by another HPLC system (column: YMC AM-312 [6.0 × 150 mm], mobile phase: ethanol/water [10/90], flow rate: 1.5 mL/min), radiochemical purity was >99%.

FLT-PET Examination

All patients were examined with a high-resolution whole-body PET scanner with an 18-ring detector arrangement (Advance; General Electric Medical Systems, Milwaukee, WI). The system permitted the simultaneous acquisition of 35 axial images with interslice spacing of 4.24 mm. Axial resolution was 4.2 mm full width at half maximum intensity, allowing multidirectional reconstruction of the images without loss of resolution.

Forty minutes after the intravenous injection of approximately 370 MBq of FLT, images of the brain were obtained. A 20-minute emission scan and 3-minute postemission transmission scan using Ge-68 source were performed. Attenuation-corrected images were reconstructed with an ordered subset expectation maximization algorithm (3 iterations and 16 subsets) with segmented attenuation correction.

Data Analysis

FLT uptake in brain lesions was semiquantitatively assessed by evaluating the standardized uptake value (SUV). Regions of interest (ROIs) were set at areas showing the highest uptake in the tumor by referring to MRI/CT images. The maximal value of SUV (SUVmax) was regarded as the representative value of each tumor. When FLT uptake in the tumor was faint and inconceivable, the ROI was set with the help of MRI/CT images. To calculate the tumor-to-normal brain uptake ratios (TNR), ROI was set on the normal brain parenchyma (mostly contralateral normal cerebral tissue excluding ventricles) and the mean value of SUV was calculated. TNR was determined by dividing the SUVmax of the tumor with the SUVmean of normal brain tissue.

The measured SUVmax and TNRs were compared with the histologic diagnoses obtained by surgery or biopsy. When the expression of Ki-67 in the tumor tissue was evaluated, the relationship between the Ki-67 index and SUVmax/TNR was evaluated.

Statistical Analysis

The Kruskal-Wallis test was used to compare the histologic grade and SUVmax/TNRs of brain gliomas. The Spearman rank correlation coefficient test was used to evaluate the relationship between Ki-67 indices and SUVmax/TNRs. P values of less than 0.05 were considered significant.

RESULTS

Normal brain parenchyma showed very weak uptake with the SUVmean ranging from 0.17 to 0.42, and FLT uptake in the tumor was detectable with good contrast except for in low-grade tumor.

In patients in group A, 3 had malignant lymphomas of diffuse large B-cell type, 3 had glioblastomas, one had a grade 3 oligodendroglioma, one had a grade 3 astrocytoma, and one had a grade 2 astrocytoma (Table 1). In patients in group B, 5 patients had glioblastomas, 2 had grade 2 astrocytomas, one had a grade 2 oligodendroglioma, one had a grade 2 ependymoma, and one had a pineal parenchymal tumor of intermediate differentiation (Table 2). For groups A and B, ie, the pretreatment evaluation of primary brain tumors, there was a significant relationship between the histologic grade and SUVmax (Fig. 1, $P = 0.0067$), in which the SUVmax increased with the increasing grade, although there was an overlap of the SUVmax between grade 2 and grade 3 tumors. Figure 2 summarizes representative cases of brain tumors of differing malignant grades. Malignant lymphomas also showed high SUVmax and TNR ranging from 3.13 to 15.48 and 12.04 to 43.94 (Fig. 3). Both glioblastomas and malignant lymphomas showed wide-ranging distribution of their SUVmax (Fig. 1).

In the 6 patients who underwent FLT-PET for the evaluation of suspected tumor recurrence (group C), all patients showed high SUVmax values (1.65–5.51) and TNRs (5.89–14.13) suggesting high-grade malignant brain tumors (Table 3). However, the histologic diagnoses were high-grade malignancy for only half of them (Fig. 4a–c), and in the remaining 3 patients, 2 had low-grade tumors (Fig. 4d–f) and one had a nontumorous lesion (granuloma) (Fig. 4g, h). For all these 3 false-positive cases, MRI (Gd-enhanced T1-weighted image) showed lesion enhancement suggestive of high-grade brain tumor.

Correlations between the malignant grade and SUVmax/TNR were reevaluated for all cases, including patients in group C, and there were significant relationships (Fig. 5, $P = 0.0208$ and 0.0132, respectively). Ki-67 indices and SUVmax/TNR could be compared for 20 cases and showed a significant relationship between them (Fig. 6, $P = 0.0070$ and 0.0079, respectively).

DISCUSSION

Noninvasive imaging and measurement of cancer cell proliferation will make it possible to evaluate the malignant

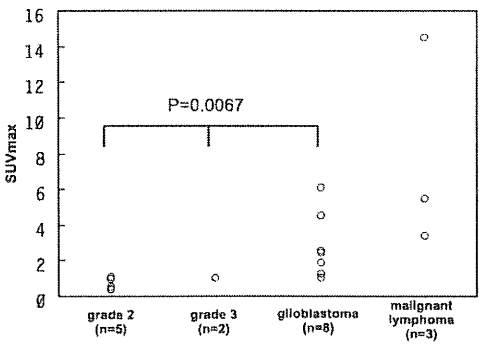

FIGURE 1. Comparison of SUVmax with the malignant grade of primary brain tumors for group A and B cases.

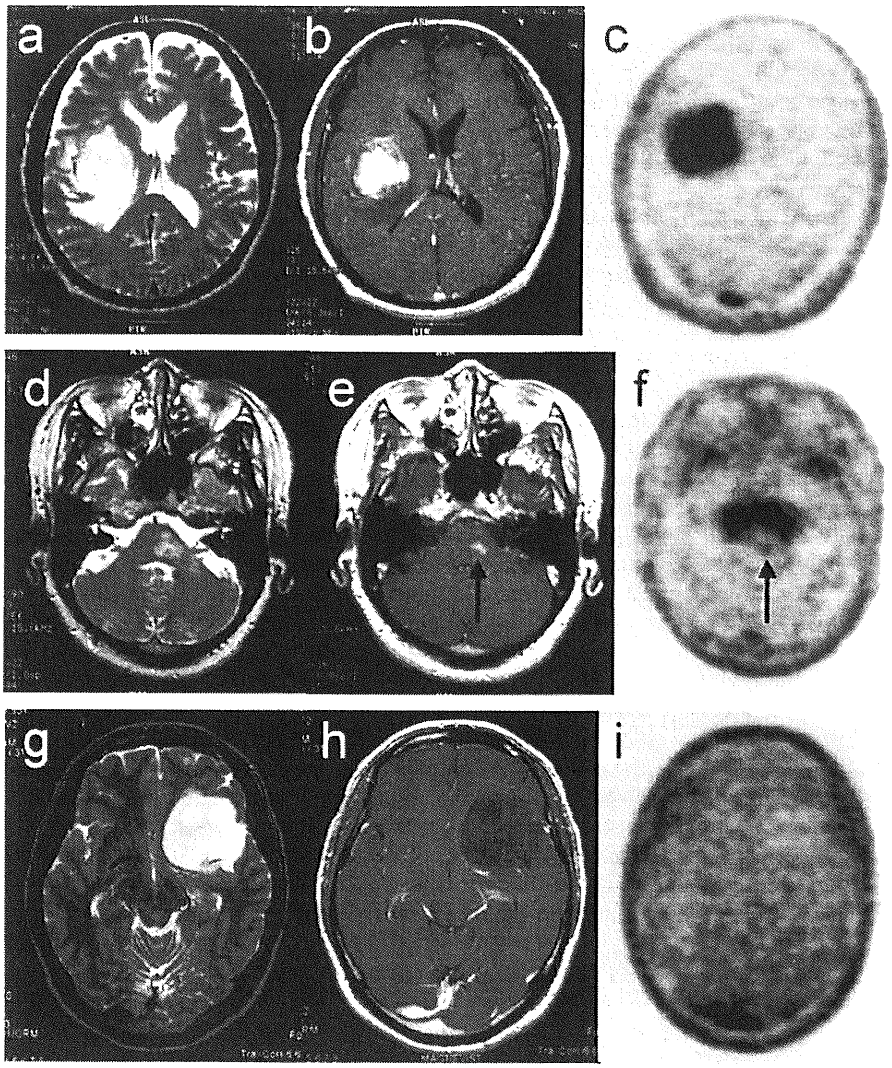

FIGURE 2. Representative cases of brain gliomas of differing grades. (a–c): A 75-year-old patient with glioblastoma. T2WI (a) shows a hyperintense mass lesion in the right cerebral hemisphere, which was strongly enhanced after the intravenous administration of Gd-DTPA (b). FLT-PET (c) shows very high uptake of FLT (SUVmax = 6.07, TNR = 20.93) in the tumor. (d–f) A 60-year-old patient with grade 3 astrocytoma. T2WI (d) shows a hyperintense brainstem lesion with focal spotty enhancement (arrow) after Gd administration (e). FLT-PET (f) shows the focal accumulation of FLT (SUVmax = 1.00, TNR = 2.86) corresponding to abnormal enhancement (arrow). (g–i): A 36-year-old patient with grade 2 astrocytoma. T2WI (g) shows a hyperintense lesion in the left frontotemporal region without abnormal enhancement after Gd administration (h). FLT-PET (i) shows no visible accumulation of FLT (SUVmax = 0.49, TNR = 1.17) corresponding to the tumor.

grade of tumors and the early response to therapy, and will also help us to differentiate malignant from benign conditions. Radiolabeled nucleoside analogs have been evaluated as proliferation markers. Among them, C-11 thymidine, which is a pyrimidine analog and is rapidly incorporated into the DNA of the proliferating cells, has been used to image proliferation.[12] However, as a result of the short half-life of C-11 and the rapid degradation of C-11 thymidine in vivo, the clinical application of C-11 thymidine is limited.[9]

Recently, an F-18-labeled pyrimidine analog, FLT, has been developed and its role as a new proliferation marker of cancer is now under extensive evaluation.[9,13] FLT is taken up by the cell by passive diffusion and/or facilitated transport and then phosphorylated by the activity of thymidine kinase

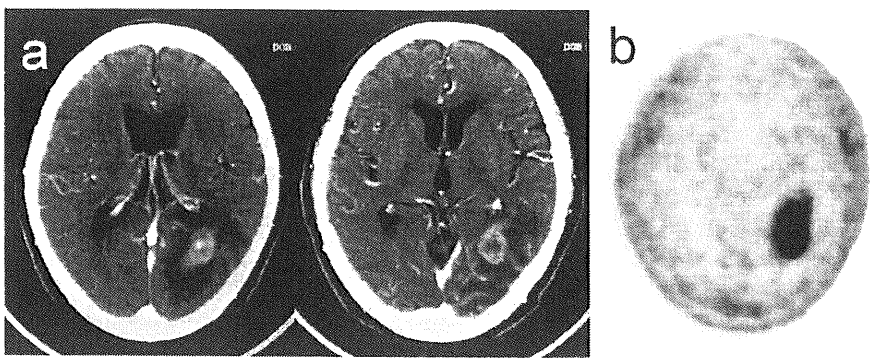

FIGURE 3. A case of malignant lymphoma of the brain. Contrast-enhanced CT of a 71-year-old patient (a) showed an enhancing mass lesion in the left temporo-occipital region suggestive of a malignant brain tumor. FLT-PET of this patient (b) showed strong FLT uptake in the tumor (SUVmax = 5.43, TNR = 18.72).

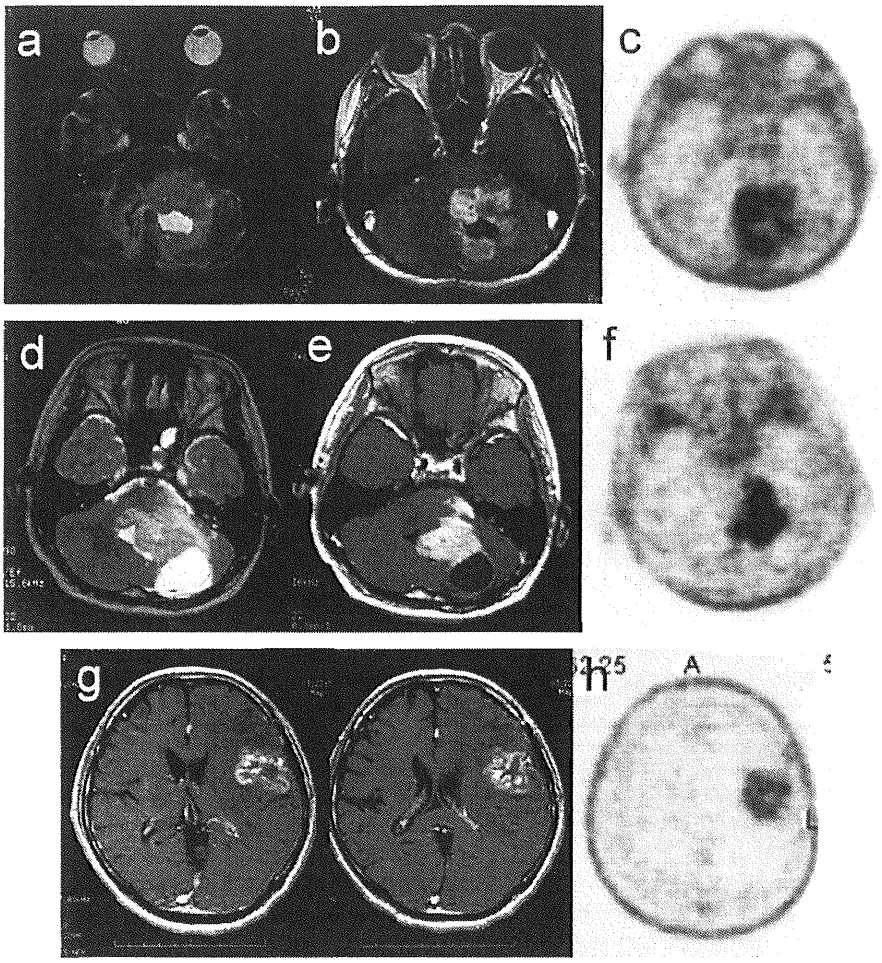

FIGURE 4. Three cases from group C. (a–c) A 54-year-old patient who underwent operation for pilocytic astrocytoma 16 months ago. Follow-up MRI showed the development of a left cerebellar tumor, which was hyperintense on T1WI (a) and was enhanced after Gd administration (b), suggestive of a high-grade malignant tumor. FLT-PET of this patient (c) showed high FLT uptake in the tumor (SUVmax = 2.09, TNR = 7.21). The patient underwent surgery and the histologic diagnosis was glioblastoma. (d–f) A 9-year-old patient underwent an operation for ganglioglioma of the cerebellum 8 months ago. He also received postoperative radiation and chemotherapy. Despite treatment, he developed a recurrent lesion, which increased in size. MRI of the brain showed a solid and cystic lesion in the left cerebellum (d) and the solid portion of the tumor showed enhancement after Gd administration (e). FLT-PET of this patient (f) showed increased FLT uptake in the solid portion of the recurrent tumor (SUVmax = 2.58, TNR = 11.22) suggestive of a high-grade malignancy. Surgery was performed and the histologic diagnosis was ganglioglioma grade 1. (g and h) A 61-year-old patient underwent an operation for glioblastoma 13 months ago followed by radiation and chemotherapy. Follow-up MRI (g) showed an enhanced lesion suggestive of recurrence and FLT-PET (h) also showed increased FLT uptake (SUVmax = 1.65, TNR = 5.89). However, surgery showed the presence of a granuloma, not a recurrent tumor.

1 (TK1) to FLT-monophosphate, which is trapped inside the cells. TK1 is involved in the salvage pathway of DNA synthesis, and the activity of TK1 is present in proliferating cells, which peaks in the late G1 and S phases.[14] Although FLT is not incorporated into DNA, in vitro and in vivo studies showed that FLT uptake reflected TK1 activity and represented the total activity of the salvage pathway.[15,16] The clinical application of FLT-PET in the evaluation of the proliferation activity of various types of cancers had been reported.[13,17–21] Recently, the application of FLT-PET for brain tumors has been reported in a few papers.[22–24]

In this investigation, we evaluated whether FLT accumulation in brain tumors can correctly predict the malignant grade and whether FLT uptake reflects the expression of the proliferation marker. First of all, unlike FDG-PET, FLT showed almost no uptake in the normal brain parenchyma giving good contrast images of brain tumors. In the low background activity of normal brain parenchyma, heterogeneous FLT uptake within the tumor area was quite obvious, suggesting the possibility of using FLT-PET to determine optimal biopsy sites showing maximal proliferation activity, ie, the highest malignant potential. In accordance with pre-

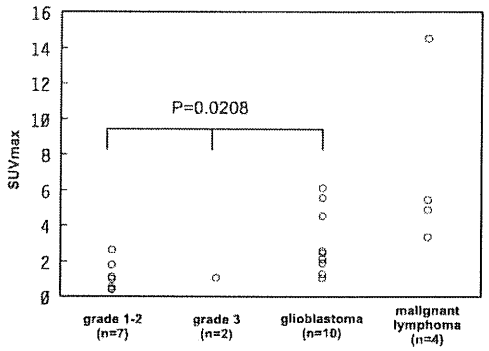

FIGURE 5. Comparison of SUVmax with the malignant grade of primary brain tumors for all cases.

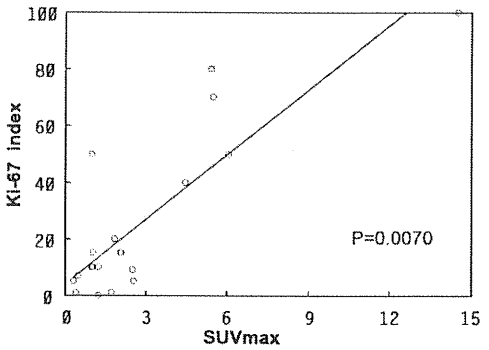

FIGURE 6. Relationships between SUVmax and Ki-67 index for all cases.

vious reports, this study showed that SUVmax and TNR were significantly correlated to the malignant grade of primary brain tumors. Although there was an overlap between grade 1 to 2 and grade 3 tumors, glioblastomas showed a higher uptake than grade 1 to 3 tumors. Furthermore, a significant relationship was observed between the SUVmax/TNR and the Ki-67 staining index. These results support the usefulness of FLT-PET in the evaluation of primary brain tumors. However, we experienced several instances of false-positive FLT uptake in low-grade brain tumors and a nontumorous lesion. All false-positive cases, 2 recurrent tumors and one granuloma, showed lesion enhancement after Gd administration, which implies a disruption of the blood–brain barrier (BBB). In evaluating radiotracer uptake in brain tumors, we need to consider the presence of the BBB in addition to tracer uptake and retention kinetics. In contrast to FDG, which shows high uptake in normal brain tissue, thymidine analogs are not transported well across the intact BBB, and disruption of the BBB appears to account for a significant proportion of the uptake phase of thymidine analogs.[25] In these 3 cases, spuriously increased FLT uptake may largely depend on BBB disruption. To further clarify these points, kinetic analysis with a dynamic study is necessary.[12,23,26] In addition, although FLT is reported to be more specific to cancerous tissues than FDG,[27] it may be accumulated in chronic granulomatous lesions with proliferative inflammation, which needs to be evaluated by animal models and by further clinical cases.

From these results, along with recent reports,[22–24] BBB disruption substantially affects FLT uptake in brain lesions. Therefore, we need to be cautious about the presence of benign brain lesions and low-grade tumors, which show BBB disruption, in evaluating enhanced brain lesions by FLT-PET. Especially in posttreatment cases, surgery and radiation therapy may cause BBB disruption and may complicate the evaluation of FLT-PET images. FLT-PET should be evaluated along with other image findings and with full clinical information. Furthermore, it is not reasonable to compare brain tumors with intact BBB with those with disrupted BBB using a single criterion (SUVmax or TNR). However, these results showed that there was a wide variation in SUVmax and TNRs among glioblastoma and malignant lymphoma cases, all of which showed contrast enhancement on MRI and/or CT. Because the BBB was disrupted in these lesions, this variation in FLT uptake seems to reflect the differences in proliferation activity. When the SUVmax/TNR of these 11 cases was compared with Ki-67 indices, there existed significant correlation ($P = 0.0080$ for both comparisons). It therefore seems that FLT-PET can be used to evaluate proliferative activity and stratify high-grade malignant brain tumors showing BBB disruption, which need to be further evaluated with more cases and prognosis correlation.

There are various limitations in this investigation. The number of patients is relatively limited, especially for grade 3 tumors. In patients in group B, histology was obtained before FLT-PET, and there is a possibility that the histologic diagnosis and/or maximal Ki-6 staining index may not correspond to the maximal SUV values. Even in preoperative cases (groups A and C), histologic diagnoses were obtained from biopsy or partial removal in a substantial number of cases. It was not possible to know whether the area showing SUVmax corresponds exactly to the area showing the highest histologic grade and/or highest number of Ki-67-positive cells, especially in large tumors with heterogeneous character. In this study, it was not possible to compare FLT-PET with other PET/SPECT tracers used for brain tumor evaluation.[3]

In conclusion, FLT-PET can be used to evaluate the malignant grade and proliferation activity of primary brain tumors, especially high-grade brain tumors. However, the presence of benign or low-grade lesions showing BBB disruption cannot be distinguished from malignant tumors and needs to be carefully evaluated.

REFERENCES

1. Ricci PE. Imaging of adult brain tumors. *Neuroimaging Clin N Am.* 1999;9:651–669.
2. Nelson SJ. Imaging of brain tumors after therapy. *Neuroimaging Clin N Am.* 1999;9:801–819.
3. Benard F, Romsa J, Hustinx R. Imaging gliomas with positron emission tomography and single-photon emission computed tomography. *Semin Nucl Med.* 2003;33:148–162.
4. Delbeke D, Martin WH. Metabolic imaging with FDG: a primer. *Cancer J.* 2004;10:201–213.
5. Wong TZ, van der Westhuizen GJ, Coleman RE. Positron emission tomography imaging of brain tumors. *Neuroimaging Clin N Am.* 2002; 12:615–626.
6. Ricci PE, Karis JP, Heiserman JE, et al. Differentiating recurrent tumor from radiation necrosis: time for re-evaluation of positron emission tomography? *AJNR Am J Neuroradiol.* 1998;19:407–413.

7. Olivero WC, Dulebohn SC, Grierson JR, et al. The use of PET in evaluating patients with primary brain tumors: is it useful? *J Neurol Nerosurg Psychiatry*. 1995;58:250–252.
8. Love C, Tomas MB, Tronco GG, et al. FDG PET of infection and inflammation. *Radiographics*. 2005;25:1357–1368.
9. Shields AF, Grierson JR, Dohmen BM, et al. Imaging proliferation in vivo with [F-18]FLT and positron emission tomography. *Nat Med*. 1998;4:1334–1336.
10. Takahashi JA, Ueba T, Hashimoto N, et al. The combination of mitotic and Ki-67 indices as a useful method for predicting short-term recurrence of meningiomas. *Surg Neurol*. 2004;61:149–156.
11. Kitano H, Magata Y, Tanaka A, et al. Performance assessment of O-18 water purifier. *Ann Nucl Med*. 2001;15:75–78.
12. Vander Borght T, Pauwels S, Lambotte L, et al. Brain tumor imaging with PET and 2-[carbon-11]thymidine. *J Nucl Med*. 1994;35:974–982.
13. Been LB, Suurmeijer AJH, Cobben DCP, et al. [^{18}F]FLT-PET in oncology: current status and opportunities. *Eur J Nucl Med Mol Imaging*. 2004;31:1659–1672.
14. Munch-Peterson B, Cloos L, Jensen K, et al. Human thymidine kinase 1. Regulation in normal and malignant cells. *Adv Enzyme Regul*. 1995;35: 69–89.
15. Rasey JS, Grierson JR, Wiens LW, et al. Validation of FLT uptake as a measure of thymidine kinase-1 activity in A549 carcinoma cells. *J Nucl Med*. 2002;43:1210–1217.
16. Barthel H, Perumal M, Latigo J, et al. The uptake of 3′-deoxy-3′-[^{18}F]fluorothymidine into L5178Y tumours in vivo is dependent on thymidine kinase 1 protein levels. *Eur J Nucl Med Mol Imaging*. 2005;32:257–263.
17. Buck AK, Schirrmeister H, Hetzel M, et al. 3-deoxy-3-[^{18}F]fluorothymidine-positron emission tomography for noninvasive assessment of proliferation in pulmonary nodules. *Cancer Res*. 2002;62:3331–3334.
18. Francis DL, Visvikis D, Costa DC, et al. Potential impact of [^{18}F]3′-deoxy-3′-fluorothymidine versus [^{18}F]fluoro-2-deoxy-D-glucose in positron emission tomography for colorectal cancer. *Eur J Nucl Med Mol Imaging*. 2003;30:988–994.
19. Buck AK, Halter G, Schirrmeister H, et al. Imaging proliferation in lung tumors with PET: ^{18}F-FLT versus ^{18}F-FDG. *J Nucl Med*. 2003;44:1426–1431.
20. Smyczek-Gargya B, Fersis N, Dittmann H, et al. PET with [^{18}F]fluorothymidine for imaging of primary breast cancer: a pilot study. *Eur J Nucl Med Mol Imaging*. 2004;31:720–724.
21. van Westreenen HL, Cobben DC, Jager PL, et al. Comparison of ^{18}F-FLT PET and ^{18}F-FDG PET in esophageal cancer. *J Nucl Med*. 2005;46:400–404.
22. Choi SJ, Kim JS, Kim JH, et al. [^{18}F]3′-deoxy-3′-fluorothymidine PET for the diagnosis and grading of brain tumors. *Eur J Nucl Med Mol Imaging*. 2005;46:945–952.
23. Chen W, Cloughesy T, Kamdar N, et al. Imaging proliferation in brain tumors with ^{18}F-FLT PET: comparison with ^{18}F-FDG. *J Nucl Med*. 2005;46:945–952.
24. Jacobs AH, Thomas A, Kracht LW, et al. ^{18}F-fluoro-L-thymidine and ^{11}C-methylmethionine as markers of increased transport and proliferation in brain tumors. *J Nucl Med*. 2005;46:1948–1958.
25. De Reuck J, Santens P, Goethals P, et al. [Methyl-^{11}C]thymidine positron emission tomography in tumoral and non-tumoral cerebral lesions. *Acta Neurol Belg*. 1999;99:118–125.
26. Muzi M, Vesselle H, Grierson JR, et al. Kinetic analysis of 3′-deoxy-3′-fluorothymidine PET studies: validation studies in patients with lung cancer. *J Nucl Med*. 2005;46:274–282.
27. van Waarde A, Cobben DC, Suurmeijer AJ, et al. Selectivity of ^{18}F-FLT and ^{18}F-FDG for differentiating tumor from inflammation in a rodent model. *J Nucl Med*. 2004;45:695–700.

Journal of Neuro-Oncology (2006) 77: 53–58
DOI 10.1007/s11060-005-7698-8

Clinical Study

Initial experiences of palliative stereotactic radiosurgery for recurrent brain lymphomas

Masato Sakamoto[1], Natsuo Oya[1,3], Takashi Mizowaki[1], Norio Araki[1], Yasushi Nagata[1], Kenji Takayama[1], Jun A Takahashi[2], Hideyuki Kano[2], Takahisa Katsuki[2], Nobuo Hashimioto[2] and Masahiro Hiraoka[1]
[1]*Department of Radiation Oncology and Image-applied Therapy, Kyoto University Graduate School of Medicine;* [2]*Department of Neurosurgery, Kyoto University Graduate School of Medicine;* [3]*Department of Radiation Oncology, Graduate School of Medical Science, Kumamoto University, Japan*

Key words: chemotherapy, recurrent PCNSL, salvage treatment, SRS, symptomatic relief, toxicity

Summary

In Kyoto University Hospital, stereotactic radiosurgery (SRS) has been performed for its rapid palliative effect in patients with recurrent primary central nervous system lymphoma (PCNSL), often in combination with salvage chemotherapy. In the present study, the treatment outcome and toxicity of SRS for recurrent PCNSL was retrospectively evaluated. Between March 1998 and June 2004, 17 histologically proven recurrent PCNSLs in nine patients were treated with linac-based stereotactic radiosurgery. All patients had developed intracranial recurrences after initial treatment including external beam radiation therapy (EBRT). The prescribed dose was 10.0–16.0 (median 12.0) Gy. Seven of nine patients received systemic chemotherapy around the time of SRS. The target volume was 0.4–24.5 ml (median 3.5 ml). Initial tumor response could be evaluated in 15 of 17 lesions. Among them, radiological complete response (CR), partial response (PR), stable disease (SD) and progressive disease (PD) was observed in 3, 10, 2, and 0 lesions, respectively. One-year overall survival rate and relapse-free survival rate after first SRS was 58% and 22%, respectively. Improvement of symptoms was observed in six patients. The time from SRS to symptomatic relief was 1–57 days (median 3 days). No ≥ grade 2 acute toxicities related to SRS were observed. In conclusion, linac-based SRS with a prescription dose of 10–12 Gy for recurrent PCNSL is useful for palliation, especially considering the short time, rapid tumor response, and low treatment toxicity.

Introduction

Primary central nervous system lymphoma (PCNSL) is a rare brain tumor entity, which accounts for 0.5–1.5% of primary intracranial neoplasms in immunocompetent individuals [1]. The natural course of untreated PCNSL is highly aggressive and fatal, with a median survival time of approximately 1.5–4 months from the time of diagnosis [2–4].

Usually, PCNSL is treated with external beam radiotherapy (EBRT) and/or chemotherapy as an initial treatment, since the radio- and chemosensitivity of PCNSL seems to be as high as that of nodal or extranodal malignant lymphomas that occur in the body. Various combined regimens such as EBRT alone [5,6], EBRT followed by CHOP-like chemotherapy [7,8], high dose intravenous methotrexate alone [9], and high dose methotrexate followed by EBRT [10–12] have been employed, showing a median survival time of 12–30 months [4–12].

Although rapid and complete tumor regression is commonly seen in most cases of PCNSL, intracranial recurrence is often observed even within the previous radiation field. Failure after initial treatment was reported in 35–60% of adequately treated patients with PCNSL [6,13–15].

The prognosis of intracranial recurrent PCNSL seems to be dismal. The median survival time has been reported to be only 2–4 months from the time of recurrence without any treatment. Patients with intracranial recurrent PCNSL may be able to be salvaged with systemic chemotherapy, and possibly with radiotherapy. Several previous reports have shown the effect of these salvage therapies on patient prognosis. Median survival time was reported to be 10–16.5 months [14–16].

The use of conventional EBRT for recurrent PCNSL is often limited in consideration of the tolerance dose of brain parenchyma. In most cases, a large volume of brain parenchyma has been irradiated as a major part of the standard initial therapy. On the other hand, stereotactic radiosurgery (SRS), which has been widely used in the treatment of various brain tumors, may be a treatment option for recurrent PCNSL. Stereotactic irradiation minimizes the irradiated volume of surrounding normal brain parenchyma. This technique delivers an effective radiation dose to the recurrent tumor without severe neurological toxicity, even when the recurrent tumor is located within the field of previous EBRT. However, the microscopic tumor infiltration is not covered by SRS alone.

In our institute, SRS has been performed for its rapid palliative effect in patients with recurrent PCNSL, often in combination with salvage chemotherapy. In the present study, the treatment outcome and toxicity of SRS for recurrent PCNSL was retrospectively evaluated.

Methods and Materials

Patient Background

Between March 1998 and June 2004, 17 histologically proven recurrent PCNSLs in nine patients were treated with linac-based stereotactic radiosurgery at Kyoto University Hospital. There were five male and four female patients and their age was 51–79 (median 66) years old at the time of the first SRS.

All patients had developed intracranial recurrences after initial treatment, including EBRT. The primary tumor lesions had received 37.8–56.0 (median 54.0) Gy using a daily dose of 1.5–2.0 Gy, in which a whole brain irradiation dose of 33.0–48.6 (median 41.4) Gy had been followed by local boost irradiation. The interval between previous EBRT and the first SRS was 6.6–50.4 (median 16.6) months.

Treatment

Corticosteroids were administered to all patients before SRS. Seven of the nine patients received systemic chemotherapy around SRS, including VEPA (vincristin, cyclophosphamide, prednisolone, adriamycin) and DeVIC (dexamethasone, etoposide, ifosfamide, carboplatin) regimens.

All patients underwent SRS using 6 MV X-ray beams generated by Clinac-2300c linear accelerator (Varian Inc., Palo Alto, CA). Treatment planning was carried out using the X-Knife system (Radionics Inc., Burlington, MA), following a 3 mm-slice contrast-enhanced CT scan and MR-CT fusion if necessary. The contrast-enhanced tumor lesions and critical structures, such as eyes, brain stem and optic nerves, were delineated. Planned target volume (PTV) was determined as the contrast-enhanced tumor with a 2–3 mm margin. Four to six beam arcs were arranged first automatically and then manually, so that the optimal dose distribution could be achieved, considering both the doses of PTV and critical structures. Irradiation was carried out in a single fraction. The prescription dose varied according to the tumor size and location. The mean prescribed dose (80% isodose) to PTV was 10.0–16.0 (median 12.0) Gy. One lesion was treated by the combination of two isocenters.

At the time of the first SRS, the number of treated tumors was one for seven patients and two for two patients. Two of the nine patients received multiple SRS sessions at the diagnosis of intracranial distant recurrences following preceding SRS; one patient received the second SRS 27 months after the first SRS, and the other received four sessions of SRS to six tumors during seven months for repeated intracranial distant recurrences.

Outcome evaluation

The patients were followed up with MRI/CT studies. Initial tumor response was evaluated within two months after SRS. In the assessment of the initial tumor response, complete response (CR), partial response (PR), progressive disease (PD), and stable disease (SD) was defined as complete disappearance of the tumor, a $\geq$ 50% reduction in the tumor volume, a $\geq$ 25% increase in the tumor volume, and non-CR/PR and non-PD, respectively.

Intracranial relapse-free survival and overall survival times were calculated from the day of the first SRS using the Kaplan–Meier method. Toxicity was judged by NCI-CTC version 2 criteria.

Neurological status of the patients was evaluated by regular interviews and physical examinations, and scored according to the RTOG functional neurological scale [17].

Results

Treatment parameters

The target volume was 0.4–24.5 (median 3.5) ml. The collimator size used was 12.5–40 (median 30) mm in diameter, and the total beam arc was 160–410 (median 395) in degree. The coverage rate of the prescription dose to PTV was 92–100 (median 99)%. The minimal and maximal tumor dose was 5.5–17.7 (median 9.1) Gy and 12.5–20.3 (median 15.2) Gy, respectively. Major treatment parameters for the 17 tumors are summarized in Table 1. In all cases, the doses to eyes, optic nerves and brain stem did not exceed 12 Gy.

Initial tumor response and local regrowth after SRS

Initial tumor response could be evaluated in 15 of 17 lesions. Among them, radiological CR, PR, SD and PD were observed in 3, 10, 2 and 0 lesions, respectively, as listed in Table 2. The overall response rate (CR plus PR) was 87%. There was no relationship between the initial tumor response and the SRS parameters, including prescription dose, minimal dose, target volume, and the coverage rate. In Figure 1, an example of CR is shown.

Local tumor regrowth was seen in one lesion, which had received a prescription dose of 12.0 Gy and a minimal dose of 6.4 Gy. It was initially judged PR, but increased in size 2.4 months after SRS.

Pattern of recurrence after SRS and survival

One patient remained disease-free for 20.3 months, one patient developed local regrowth 2.4 months after SRS, and seven patients developed intracranial distant recurrences 0.7–27.2 (median 3.1) months after the first SRS. Recurrences after the first SRS were salvaged by further SRS in two patients, and by systemic chemotherapy in three patients.

One-year overall survival rate and one-year intracranial relapse-free survival rate was 58% and 22%, respectively, as shown in Figure 2. Median overall survival time and median intracranial relapse-free survival time was 7.7 months and 3.7 months, respectively. No relationship between the SRS parameters and survival was observed in the present study. However, the median overall survival time in patients with peri-SRS chemotherapy was significantly longer than that in patients

Table 1. Patient characteristic and treatment parameter of SRS

Patients	Sex	Lesion number	Location	Age at SRS (y.o.)	Time between EBRT and SRS (month)	Lesion volume (ml)	Isocenter/Prescription dose (Gy)	Max / Min dose (Gy)
1	F	1	lt. Frontal lobe	57	16.6	9.4	20.0 / 16.0	20.3 / 17.7
2	M	1	rt. Thalamus	62	29.1	5.3	15.0 / 12.0	15.8 / 12.7
		2	lt. Internal capsule	62	29.1	1.0	15.0 / 12.0	17.4 / 11.6
3	M	1	lt. Temporo-occipital lobe	66	50.4	7.8	15.0 / 12.0	15.3 / 13.5
4	F	1	rt. Parietal lobe	64	33.8	18.5	15.0 / 12.0	15.2 / 6.4
5	M	1	rt. Frontal lobe	79	10.2	1.8	15.0 / 12.0	15.0 / 12.9
6	F	1	Cerebellum	67	6.6	14.6	15.0 / 12.0	17.5 / 7.8
7	F	1	rt. Lateral ventricle	71	16.6	1.1	15.0 / 12.0	15.0 / 13.6
		2	lt. Occipital lobe	73	43.9	4.9	15.0 / 12.0	15.3 / 13.8
8	M	1	rt. Frontal lobe	51	12.8	14.9	12.5 / 10.0	13.0 / 5.5
		2	Brain stem	51	12.8	24.5	12.5 / 10.0	15.6 / 6.4
9	M	1	rt. Insula	69	37.1	2.7	15.0 / 12.0	15.0 / 7.1
		2	rt. Temporal lobe	69	38.4	1.8	15.0 / 12.0	15.0 / 12.3
		3	lt. Occipital lobe	69	38.4	0.4	15.0 / 12.0	15.2 / 9.0
		4	lt. Lateral ventricle	69	39.4	2.3	12.5 / 10.0	12.5 / 9.1
		5	rt. Basal ganglia	69	41.6	3.5	12.5 / 10.0	12.9 / 7.9
		6	Fourth ventricle	69	41.6	0.4	12.5 / 10.0	12.9 / 7.4

without peri-SRS chemotherapy (5.9 vs. 13.0 months, $P = 0.046$), as shown in Figure 3.

Palliative effects

Eight of the nine patients had symptoms possibly resulting from recurrent tumors before the first SRS. For six of these patients, symptomatic relief was achieved; in five patients the motor function was improved, and in the other patient the frequency of convulsion was remarkably decreased.

Comparing the scores in the RTOG functional neurological scale before and after the first SRS, improvement in the neurological status was observed in five of the nine patients, as shown in Table 2.

The time from SRS to symptomatic relief was 1–57 (median 3) days.

Toxicity

No ≥ grade 2 acute toxicities related to SRS were observed, although three of the nine patients developed grade 3 bone marrow toxicity due to peri-SRS systemic chemotherapy.

Discussion

The role of SRS in the treatment of PCNSL has not been established. In several institutions, SRS is often

Table 2. Treatment results of SRS (Initial tumor response and symptomatic improvement)

Patients	Sex	Lesion number	Location	Initial tumor response	Symptomatic improvement after first SRS	Functional neurological level change	Survival time after first SRS (month)
1	F	1	lt. Frontal lobe	PR	(+) decreasing frequency of convulsions	4 → 4	6.6
2	M	1	rt. Thalamus	SD	(−)	4 → 4	14.9
		2	lt. Internal capsule	SD			
3	M	1	lt. Temporo-occipital lobe	PR	(+) improving gait disturbance and disorientation	1 → 0	20.3
4	F	1	rt. Parietal lobe	PR	(+) improving gait disturbance	4 → 3	5.5
5	M	1	rt. Frontal lobe	CR	(+) improving gait disturbance and eye movement	3 → 2	6.3
6	F	1	Cerebellum	CR	(−)	4 → 4	2.1
7	F	1	rt. Lateral ventricle	CR	(+) improving results of MMT	2 → 1	47.8
		2	lt. Occipital lobe	PR			
8	M	1	rt. Frontal lobe	PR	(+) improving eye movement, diplopia and gait disturbance	2 → 1	13.0
		2	Brain stem	PR			
9	M	1	rt. Insula	PR	(−)	0 → 0	7.7
		2	rt. Temporal lobe	PR			
		3	lt. Occipital lobe	PR			
		4	lt. Lateral ventricle	PR			
		5	rt. Basal ganglia	?			
		6	Fourth ventricle	?			

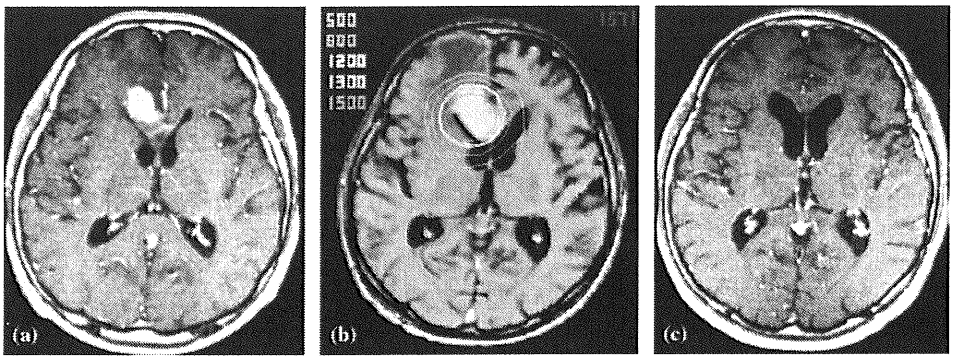

Figure 1. A case with recurrent PCNSL treated with SRS. A 51-year-old man with multiple intracranial recurrent tumors approximately one year after initial treatment. At first, several courses of salvage chemotherapy were attempted, but two of the tumors were resistant to chemotherapy (rt. frontal lobe and brain stem). Cranial nerve palsy and gait disturbance were progressive. Palliative SRS was performed at a prescription dose of 10 Gy. (a) MR image at the time of SRS, (b) treatment planning, (c) MR image three months after SRS.

performed in the initial treatment of newly diagnosed PCNSL, when strong and rapid localized effects are expected. For elderly patients with PCNSL, for whom EBRT or chemotherapy cannot be safely performed, SRS alone may be indicated as a treatment option [11,18]. However, considering the dose distribution character of SRS and the infiltrative and intracranial migration-prone nature of PCNSL, SRS has been generally used as part of the initial treatment combined with EBRT and/or chemotherapy, if treated with curative intent [15,16,19].

In other institutions, SRS for PCNSL has been mainly performed for palliation. In our institution, newly diagnosed PCNSL is usually treated with chemotherapy followed by EBRT, and recurrent PCNSL is treated with SRS with or without chemotherapy, in patients with symptomatic intracranial recurrence, whose neurological symptoms may be improved by tumor volume reduction. So far, however, only a few previous papers have shown the outcome of SRS in this use. Therefore, we evaluated the treatment effects and toxicity of SRS for recurrent PCNSL and reported our initial experiences.

Recurrent brain tumors, including gliomas, meningiomas, and metastatic brain tumors, are also treated with SRS, when they recurred after full dose EBRT. However, in most cases, a relatively high SRS dose is required to achieve tumor regression and/or symptomatic improvement [20–23]. On the other hand, it is expected that recurrent PCNSL remains radiosensitive, compared with the other recurrent brain tumor entities. In the present study, a prompt and drastic response even to a lower SRS dose was demonstrated.

With respect to the SRS dose, 18–24 Gy (as the isocenter dose of stereotactic radiotherapy) [11] and 12.5–23 Gy (as the marginal dose of gamma-knife) [18] were used in the previous reports. The prescription dose of 10–12 Gy used in the present series seems to be adequate for recurrent PCNSL, considering that all of the 17 lesions, except two lesions in patient 2, showed tumor regression. In addition, no SRS-related toxicity was observed, suggesting that an SRS dose of 10–12 Gy could be safely given after a full dose of EBRT, even for patients with recurrent PCNSL adjacent to the brain stem or optic nerves.

In the present series, only one large tumor lesion in patient 4 developed local regrowth. The tumor volume of this lesion was 18.5 ml at the time of SRS, and the minimum dose was as low as 6.4 Gy, while the prescription dose (12 Gy) coverage was 97%. This lesion once showed tumor regression associated with good palliative effects, but developed local regrowth 2.4 months after SRS. Although the focus of tumor regrowth could not be identified, it was probable that the existence of a small part of the tumor irradiated with an

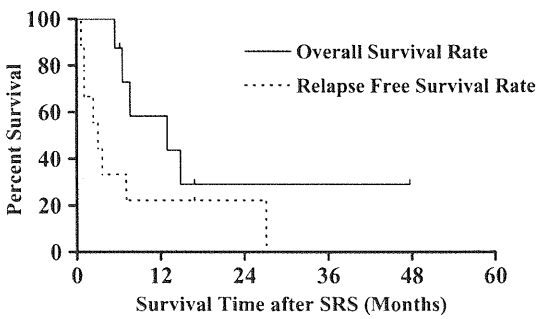

Figure 2. Graph showing Kaplan–Meier estimate of overall survival rate (——) and relapse-free survival rate (- - - - -) in all patients after the first SRS for recurrent PCNSL (median survival, 7.7 and 3.3 months, respectively).

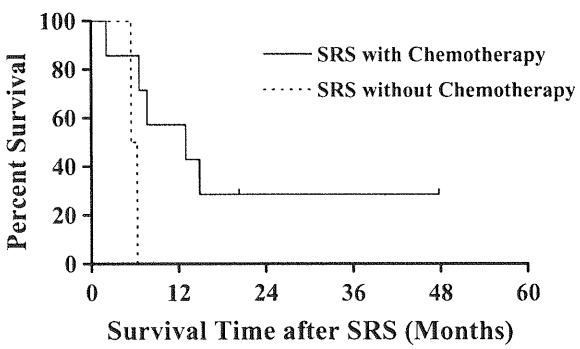

Figure 3. Graph showing Kaplan–Meier estimate of survival rate comparison after the first SRS for recurrent PCNSL between the patients treated SRS with chemotherapy (——, $n = 7$) versus the patients treated SRS without chemotherapy (- - - - -, $n = 2$). Median overall survival was longer in the SRS with chemotherapy cohort (13.0 months) than the SRS without chemotherapy cohort (5.9 months) ($P = 0.046$).

insufficient dose might have resulted in the local regrowth.

Symptomatic relief was achieved in six of eight cases, as expected, which demonstrated the excellent usefulness of SRS as a palliative indication. In addition, a considerably prompt response (median 3 days) should be noted as an advantage of SRS.

With respect to the survival time, one-year- and two-year-survival after the first SRS, were 58% and 22%, respectively, and the median survival time after the first SRS was 7.7 months in all patients and 13.6 months in the patients treated with chemotherapy in the present series. These results were slightly inferior to those of the salvage treatments using systemic chemotherapy and/or radiation therapy for recurrent PCNSL in a previous report, in which the median survival time was reported to be 14 months [14,15]. Considering the expected lifetime of only 2–4 months for patients with non-treated recurrent PCNSL [14,15], the results in the present series also demonstrated the survival benefit of SRS in patients with recurrent PCNSL.

Various regimens of systemic chemotherapy are often chosen for patients with recurrent PCNSL. Several previous reports have shown promising treatment response [16,24–26].

Arellano-Rodrigo et al. [16] reported that CR was obtained in six of sixteen cases (37%) and one-year survival was 41% with etoposide, ifosfamide, and cytarabine treatment. However, toxicity consisted of neutropenic fever in 50% of cases, including three cases of sepsis and two cases of pneumonia. In addition, severe encephalopathy was observed in one case. Soussain et al. [24] reported the results of a phase II study of 22 patients treated with intensive chemotherapy with hematopoietic stem-cell rescue. In that study, an objective response was seen in 82%, and the overall three year survival was 64%. On the other hand, after intensive chemotherapy with hematopoietic stem-cell rescue, all patients had grade 4 neutropenia and grade 4 thrombocytopenia. In addition, there was possibility that five of seven patients $\geqslant$ 60 years of age died from treatment complications. Reni et al. [25] reported the results that median survival for all patients was 3.5 months (range 0.4–43 months). One year overall survival was 38%. There were five CR in 23 evaluable patients. But CR occurred after two cycles of temozolomide in four patients and after ten cycles in one patient. Three CR patients received four cycles of temozolomide, one patient eight cycles and one patient twelve cycles. Enting et al. [26] reported the treatment outcome with rituximab and temozolomide as a 53% response rate, median overall survival of 14 months, and median progression free survival of 7.7 months, while there was a 20–30% grade 3 hematologic toxicity (in 15 patients, grade 3 thrombocytopenia was seen in four patients, grade 3 anemia in one and grade 3 leukopenia in one).

It is difficult to compare simply the treatment outcome of chemotherapy and that of SRS, because the treatment modality is usually selected according to the tumor size, location and distribution in individual patients. However, particularly for palliative indication, SRS seems to have several advantages over systemic chemotherapy, even though the contribution of SRS to the survival benefit was not revealed clearly in the present study. First, the treatment time of SRS, usually a couple of days, is much shorter than that of effective chemotherapy, which requires several days or weeks. Second, more prompt symptomatic relief may be expected by SRS compared with chemotherapy. Third, SRS is usually performed without systemic toxicity, including hematological toxicity, which may potentially prolong the time of hospitalization. Therefore, SRS is suited for the palliative intent, if it is expected that volume reduction of recurrent PCNSL may provide symptomatic relief.

In patients with a good prognosis, combination of SRS and systemic chemotherapy seems to be indicated. In the present study, six out of nine patients received chemotherapy. The median survival time of the six patients was longer than that of the three patients treated with SRS alone, although there was treatment selection bias.

In conclusion, *linac*-based SRS with a prescription dose of 10–12 Gy for recurrent PCNSL is useful for palliation, especially considering the short treatment time, rapid tumor response, and low treatment-related toxicity. Although the survival benefit of SRS for recurrent PCNSL was unclear, the combination of SRS and chemotherapy may be an effective strategy for better clinical outcome. This optimal treatment regimen of combined therapy for recurrent PCNSL should be established.

References

1. Fine HA, Mayer RJ: Primary central nervous system lymphoma. Ann Intern Med 119: 1093–1104, 1993
2. Plotkin SR, Batchelor TT: Primary nervous-system lymphoma. Lancet Oncol 2: 354–365, 2001
3. Ferreri AJ, Abrey LE, Blay JY, Borisch B, Hochman J, Neuwelt EA, Yahalom J, Zucca E, Cavalli F, Armitage J, Batchelor T: Summary statement on primary central nervous system lymphomas from the Eighth International Conference on Malignant Lymphoma, Lugano, Switzerland, June 12 to 15, 2002. J Clin Oncol 21: 2407–2414, 2003
4. van der Sanden GA, Schouten LJ, van Dijck JA, van Andel JP, van der Maazen RW, Coebergh JW, Working Group of Specialists in Neuro-Oncology in the Southern, Eastern Netherlands: Primary central nervous system lymphomas: incidence and survival in the Southern and Eastern Netherlands. Cancer 94: 1548–1556, 2002
5. Ishikawa H, Hasegawa M, Tamaki Y, Hayakawa K, Akimoto T, Sakurai H, Mitsuhashi N, Niibe H, Tamura M, Nakano T: Comparable outcomes of radiation therapy without high-dose methotrexate for patients with primary central nervous system lymphoma. Jpn J Clin Oncol 33: 443–449, 2003
6. Shibamoto Y, Tsuchida E, Seki K, Oya N, Hasegawa M, Toda Y, Takemoto M, Sumi M, Hiratsuka J, Oguchi M, Hosono M, Yasuda S, Sougawa M, Kakutoh Y, Hayabuchi N: Primary central nervous system lymphoma in Japan 1995–1999: changes from the preceding 10 years. J Cancer Res Clin Oncol 130: 351–356, 2004
7. Bessell EM, Lopez-Guillermo A, Villa S, Verger E, Nomdedeu B, Petit J, Byrne P, Montserrat E, Graus F: Importance of radiotherapy in the outcome of patients with primary CNS lymphoma: an analysis of the CHOD/BVAM regimen followed by two different radiotherapy treatments. J Clin Oncol 20: 231–236, 2001

8. Bessell EM, Graus F, Lopez-Guillermo A, Villa S, Verger E, Petit J, Holland I, Byrne P: CHOD/BVAM regimen plus radiotherapy in patients with primary CNS non-Hodgkin's lymphoma. Int J Radiat Oncol Biol Phys 50: 457–464, 2001
9. Cheng T, Forsyth P, Chaudhry A, Morris D, Gluck S, Russell JA, Stewart DA: High-dose thiotepa, busulfan, cyclophosphamide and ASCT without whole-brain radiotherapy for poor prognosis primary CNS lymphoma. Bone Marrow Transplant 31: 679–685, 2003
10. Poortmans PM, Kluin-Nelemans HC, Haaxma-Reiche H, Van't Veer M, Hansen M, Soubeyran P, Taphoorn M, Thomas J, Van den Bent M, Fickers M, Van Imhoff G, Rozewicz C, Teodorovic I, van Glabbeke M, European Organization for Research, Treatment of Cancer Lymphoma Group: High-dose methotrexate-based chemotherapy followed by consolidating radiotherapy in non-AIDS-related primary central nervous system lymphoma: European Organization for Research and Treatment of Cancer Lymphoma Group Phase II Trial 20962. J Clin Oncol 21: 4483–4488, 2003
11. Watanabe T, Katayama Y, Yoshino A, Komine C, Yokoyama T, Fukushima T: Long-term remission of primary central nervous system lymphoma by intensified methotrexate chemotherapy. J Neurooncol 63: 87–95, 2003
12. Plasswilm L, Herrlinger U, Korfel A, Weller M, Kuker W, Kanz L, Thiel E, Bamberg M: Primary central nervous system (CNS) lymphoma in immunocompetent patients. Ann Hematol 81: 415–423, 2002
13. Shibamoto Y, Hayabuchi N, Hiratsuka J, Tokumaru S, Shirato H, Sougawa M, Oya N, Uematsu Y, Hiraoka M: Is whole-brain irradiation necessary for primary central nervous system lymphoma? Patterns of recurrence after partial-brain irradiation. Cancer 97: 128–133, 2003
14. Reni M, Ferreri AJ, Villa E: Second-line treatment for primary central nervous system lymphoma. Br J Cancer 79: 530–534, 1999
15. Reni M, Ferreri AJ: Therapeutic management of refractory or relapsed primary central nervous system lymphomas. Ann Hematol 80(Suppl 3): B113–117, 2001
16. Arellano-Rodrigo E, Lopez-Guillermo A, Bessell EM, Nomdedeu B, Montserrat E, Graus F: Salvage treatment with etoposide (VP-16), ifosfamide and cytarabine (Ara-C) for patients with recurrent primary central nervous system lymphoma. Eur J Haematol 70: 219–224, 2003
17. Radiation Therapy Oncology Group: RTOG 95-07 Phase I Study OF Topotecan Plus Cranial Radiation for Glioblastoma Multiforme (NSC #609699) Appendix II Neurologic Function (NF) Status
18. Dong Y, Pan L, Wang B, Wang E, Zhang N, Cai P, Dai J: Stereotactic radiosurgery in the treatment of primary central nervous system lymphoma. Chin Med J (Engl) 116: 1166–1170, 2003
19. Tyson RM, Siegal T, Doolittle ND, Lacy C, Kraemer DF, Neutwelt EA: Current status and future of relapsed primary central nervous system lymphoma (PCNSL). Leuk Lymphoma 44: 627–633, 2003
20. Stafford SL, Pollock BE, Foote RL, Gorman DA, Nelson DF, Schomberg PJ: Stereotactic radiosurgery for recurrent ependymoma. Cancer 88: 870–875, 2000
21. Hudes RS, Corn BW, Werner-Wasik M, Andrews D, Rosenstock J, Thoron L, Downes B, Curran WJ Jr: A phase I dose escalation study of hypofractionated stereotactic radiotherapy as salvage therapy for persistent or recurrent malignant glioma. Int J Radiat Oncol Biol Phys 43: 293–298, 1999
22. Alexander E III, Loeffler JS: Radiosurgery for primary malignant brain tumors. Semin Surg Oncol 14: 43–52, 1998
23. Varlotto JM, Flickinger JC, Niranjan A, Bhatnagar AK, Kondziolka D, Lunsford LD: Analysis of tumor control and toxicity in patients who have survived at least one year after radiosurgery for brain metastases. Int J Radiat Oncol Biol Phys 57: 452–464, 2003
24. Soussain C, Suzan F, Hoang-Xuan K, Cassoux N, Levy V, Azar N, Belanger C, Achour E, Ribrag V, Gerber S, Delattre JY, Leblond V: Results of intensive chemotherapy followed by hematopoietic stem-cell rescue in 22 patients with refractory or recurrent primary CNS lymphoma or intraocular lymphoma. J Clin Oncol 19: 742–749, 2001
25. Reni M, Mason W, Zaja F, Perry J, Franceschi E, Bernardi D, Dell'Oro S, Stelitano C, Candela M, Abbadessa A, Pace A, Bordonaro R, Latte G, Villa E, Ferreri AJ: Salvage chemotherapy with temozolomide in primary CNS lymphomas: preliminary results of a phase II trial. Eur J Cancer 40: 1682–1688, 2004
26. Enting RH, Demopoulos A, DeAngelis LM, Abrey LE: Salvage therapy for primary CNS lymphoma with a combination of rituximab and temozolomide. Neurology 63: 901–903, 2004

Address for offprints: Masato Sakamoto, M.D., Department of Radiation Oncology and Image-applied Therapy, Kyoto University Graduate School of Medicine, 54 Shogoin-Kawaharacho Sakyo-ku, Kyoto, Japan; Tel: +81-75-751-3419; Fax: +81-75-771-9749; E-mail: skmt@kuhp.kyoto-u.ac.jp

Cervical Lymph Node Metastases: Diagnosis at Sonoelastography—Initial Experience[1]

Andrej Lyshchik, MD, PhD
Tatsuya Higashi, MD, PhD
Ryo Asato, MD, PhD
Shinzo Tanaka, MD, PhD
Juichi Ito, MD, PhD
Masahiro Hiraoka, MD, PhD
Michael F. Insana, PhD
Aaron B. Brill, MD, PhD
Tsuneo Saga, MD, PhD
Kaori Togashi, MD, PhD

Purpose: To prospectively estimate the accuracy of sonoelastography in the differentiation of benign and metastatic cervical lymph nodes (LNs) in patients suspected of having thyroid or hypopharyngeal cancer, with histologic nodal findings as the reference standard.

Materials and Methods: The study protocol was approved by the hospital review board; each patient gave written informed consent. One hundred forty-one peripheral neck LNs (60 metastatic, 81 metastasis free) in 43 consecutive patients (22 men, 21 women; mean age, 58 years ± 13 [standard deviation]) were examined. Patients referred for surgical treatment of suspected thyroid or hypopharyngeal cancer were examined with gray-scale ultrasonography (US), power Doppler US, and sonoelastography. At gray-scale and power Doppler US, the following LN characteristics were evaluated: short-axis diameter, short-to-long-axis diameter ratio, echogenicity, calcifications, and vascularity. A four-point rating scale was used to evaluate the US elastograms for LN visibility, relative brightness, margin regularity, and margin definition. In addition, strains of LN and surrounding neck muscles were measured on elastograms, and the muscle-to-LN strain ratio—that is, the strain index—was calculated. The diagnostic potential of the examined criteria for metastatic involvement was evaluated with univariate analysis and multivariate generalized estimating equation (GEE) regression. $P < .05$ indicated statistical significance.

Results: A strain index greater than 1.5 had high utility in metastatic LN classification, with 98% specificity, 85% sensitivity, and 92% overall accuracy. These results were significantly better than those obtained by using the best gray-scale criterion—that is, a short-to-long-axis diameter ratio greater than 0.5—which had 81% specificity, 75% sensitivity, and 79% overall accuracy.

Conclusion: Sonoelastography had high accuracy (92%) in the differentiation of benign and metastatic cervical LNs in patients suspected of having thyroid or hypopharyngeal cancer.

[1] From the Departments of Diagnostic Imaging and Nuclear Medicine (A.L., T.H., T.S., K.T.), Otolaryngology–Head and Neck Surgery (R.A., S.T., J.I.), and Therapeutic Radiology and Oncology (M.H.), Kyoto University Graduate School of Medicine, Sakyo-ku, Kyoto 606-8507, Japan; Beckman Institute for Advanced Science and Technology, University of Illinois, Urbana, Ill (M.F.I.); and Department of Radiology and Radiological Sciences, Vanderbilt University, Nashville, Tenn (A.B.B.). Received December 13, 2005; revision requested January 25, 2006; revision received March 22; accepted April 20; final version accepted July 17. Supported by grant-in-aid #17659366 from the Ministry of Education, Culture, Sports, Science and Technology of Japan. **Address correspondence to** A.L., Department of Radiology and Radiological Sciences, Vanderbilt University Medical Center, CCC-1118 MCN, 1161 21st Ave, South Nashville, TN 37232-2675 (e-mail: *Andrej.lyshchik@vanderbilt.edu*).

Evaluation of cervical lymph nodes is an important procedure for patients with thyroid or hypopharyngeal cancers because the results influence the prognosis and the choice of therapy (1–3). In these patients, ultrasonography (US) can be used to assess the location, number, size, internal characteristics, and vascularity of cervical lymph nodes. However, the US criteria for metastatic lymph nodes are controversial (4,5).

Sonoelastography is an imaging modality used to map the elastic properties of examined soft tissues (6). Because the elasticity of biologic tissues cannot be measured directly, the majority of the proposed elastographic techniques involve an indirect approach to estimating tissue stiffness. Briefly, mechanical stimuli of some kind (compression or vibration) are propagated into the tissue, and the resultant strain distribution is detected and characterized by using a conventional imaging technique such as US (7,8). The results of the tissue compression are displayed as an image called an elastogram, on which stiff areas appear dark and soft areas appear bright. Although sonoelastography is not yet used in routine clinical practice, it has been shown to be useful in the differential diagnosis of breast, thyroid, and prostate cancers (9–11). Our recent study results showed that sonoelastography is a promising imaging technique that can provide assistance in the differentiation of benign and metastatic thyroid tumors (10). However, to our knowledge, sonoelastography has not been applied to lymph node characterization.

Neck lymph nodes are well positioned for elastographic examination: They are easily accessible and can be efficiently compressed against underlying anatomic structures with use of a US probe. The information on lymph node stiffness would seem to be clinically useful for guidance of percutaneous biopsy and/or nodal dissection. Use of this information can also improve patient follow-up by enabling detection of cancer recurrence (depicted as stiffness) at early stages. Thus, the aim of our study was to prospectively estimate the accuracy of sonoelastography in the differentiation of benign and metastatic cervical lymph nodes in patients suspected of having thyroid or hypopharyngeal cancer, with histologic nodal findings as the reference standard.

Advance in Knowledge

- We found sonoelastography to have high accuracy (92%) in the differentiation of benign and metastatic cervical lymph nodes in patients suspected of having thyroid or hypopharyngeal cancer.

Materials and Methods

To perform our study, a kit used to modify the output from the Sonoline Elegra US scanner (Siemens Medical Systems, Issaquah, Wash) was loaned to us from the manufacturer. However, the authors had full control over the data and information submitted for publication.

Patients

The study was conducted at Kyoto University Hospital during a 12-month period: from January through December 2005. The study protocol was approved by the institutional review board. Before enrollment, each patient gave written informed consent, as required by the Kyoto University Human Study Committee. The inclusion criterion was preoperative suspicion of thyroid or hypopharyngeal cancer based on clinical, imaging, and cytologic findings. Patients who refused to give informed consent or who did not undergo surgical treatment were excluded from the study. All patients included in our study underwent surgery, and the final diagnosis was based on the results of histologic examination of the resected specimens.

A total of 47 patients (23 men, 24 women; mean age, 58 years ± 13 [standard deviation]; range, 32–85 years) were referred for our study. Four patients (one man, three women) were excluded owing to a lack of informed consent for sonoelastography. The remaining 43 consecutive patients (22 men, 21 women; mean age, 58 years ± 13; range, 32–85 years) who met the inclusion criteria were included in this prospective study (Fig 1).

US Examinations

In all patients, gray-scale and power Doppler US was performed by using the Sonoline Elegra scanner and a 7.5-MHz linear probe (Siemens Medical Systems). The US images obtained in each patient were acquired, reviewed, and interpreted by two radiologists (A.L., T.H.) together. All interpretations were performed before surgery, and the readers were blinded to the patients' final diagnoses. Before the study, the radiologists agreed on the methods of image acquisition and interpretation. Decisions regarding the findings were reached by consensus. The first investigator (A.L.) had 7 years of experience performing US for cervical lymph node diagnosis, and the second investigator (T.H.) had 16 years of this experience.

For all patients, the US examination started with gray-scale imaging. The positioning of the patients for imaging was identical to that used for standard clinical neck US: The patient was positioned on his or her back with the neck slightly extended over a pillow. During gray-scale US, lymph nodes were identified, electronic calipers were used to measure the nodes in three planes, and a region of interest for sonoelastography was identified. The size of the gray-scale images was 40 mm in depth and 40 mm in lateral width; the size of the region of interest for sonoelastography was 35

Published online before print
10.1148/radiol.2431052032

Radiology 2007; 243:258–267

Abbreviation:
CI = confidence interval

Author contributions:
Guarantors of integrity of entire study, A.L., T.H.; study concepts/study design or data acquisition or data analysis/interpretation, all authors; manuscript drafting or manuscript revision for important intellectual content, all authors; manuscript final version approval, all authors; literature research, A.L.; clinical studies, all authors; statistical analysis, A.L.; and manuscript editing, A.L., T.H., A.B.B.

Authors stated no financial relationship to disclose.

mm in depth and 30 mm in lateral width. At gray-scale US, the following US characteristics of the examined lymph nodes were evaluated: short-axis diameter and short-to-long-axis diameter ratio in the longitudinal plane with respect to the patient's neck, echogenicity, and presence of micro- or macrocalcifications (12). Lymph nodes were assessed for echogenicity with respect to the surrounding muscles and classified as hypoechoic, isoechoic, or hyperechoic. The lymph node hilum, which normally appears as a hyperechoic region (13), was excluded in this assessment.

At power Doppler US, the type and intensity of nodal blood flow were evaluated for all examined lymph nodes. Two types of lymph node vascularity were identified: In type 1, flow signals were absent or the blood flow was limited to the lymph node hilum. In type 2, there was increased peripheral blood flow (14). Doppler amplification was controlled so that the surrounding tissues displayed minimal noise.

Radiofrequency Image Acquisition and Off-line Strain Image Reconstruction

After gray-scale and power Doppler US, both examiners (A.L., T.H.) acquired a separate new set of radiofrequency echo data for sonoelastography for each lymph node. Before image acquisition, light compression (precompression) was applied, with use of the US probe, to the anterior part of the neck above the examined lesion to fix the position of the lymph node and limit its lateral movement. Then, a second light compressive force (main compression) was applied to the same area. During the steady increase in compressive force, a total of 26 images were acquired at a speed of 16 frames per second. After acquisition, the radiofrequency images were stored in the scanner's memory and then exported to an external personal computer for off-line processing. Preparation for the radiofrequency image acquisitions, including region of interest selection and lymph node precompression, required 1–2 minutes; the radiofrequency image acquisitions required 1–2 seconds; and image storage and transfer required 2–3 minutes of examination time. The precompression and the main compression were applied by using a freehand technique, without measurement of the actual force applied to the US transducer.

Strain images were processed from the original radiofrequency data by using cross-correlation algorithms (15,16). These algorithms were identical to the algorithm used in our previous study for off-line elastographic imaging of thyroid gland tumors (10). Of the two acquired sets of strain images for each examined lymph node, only the image set that had the lowest amount of noise and decorrelation artifacts (due to lateral and out-of-plane motion) was selected for final analysis. The strain image set to be used for final analysis was selected by consensus. From 26 successive frames taken for each nodule, we generated 25 displacement images by comparing the neighboring frames. The derivative of each displacement image was calculated to be the initial strain image.

After the calculation of the initial strain images, an "averaged" elastogram was formed by averaging successful initial strain images in the strain series. To obtain compatible results of relative strain values between patients, we normalized each elastogram by first subtracting the average strain, before averaging. The image-processing software averaged the shift and the strain and then discarded them before displaying the image. To improve the quality of the final averaged elastograms, frames affected by a substantial amount of noise and decorrelation artifacts on the lymph node and/or the surrounding muscle areas were excluded from the series. The images that would be excluded from the series were selected by consensus. For all patients, strain image processing was performed by the same radiologist (A.L.). Reconstruction of one set of strain images usually required 30–40 minutes of computer processing time.

The final averaged elastogram for each examined lymph node was evaluated with use of the following qualitative criteria, which were assessed by using a four-point scale: For lymph node visualization, a rating of not visible, barely visible, partially visible, or very visible was assigned. For relative lymph node brightness with respect to the surrounding neck muscles, a classification of very dark, substantially darker than surrounding muscle, slightly darker than surrounding muscle, or same brightness as or brighter than surrounding muscle was assigned. For regularity of the outline of the lymph node margin with respect to smoothness of the lymph node

Figure 1

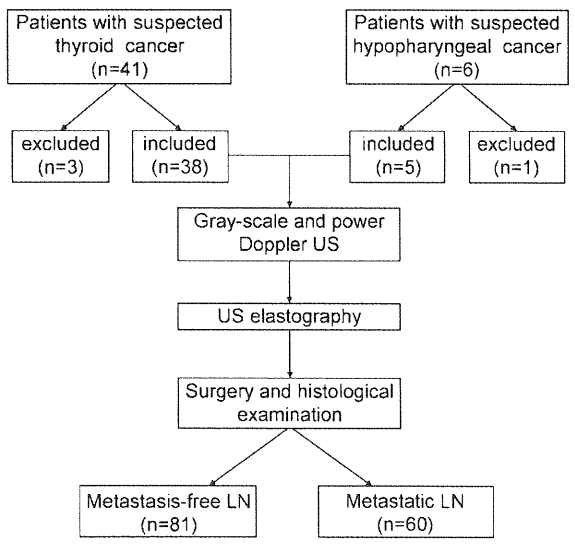

Figure 1: Patient flow diagram. *LN* = lymph node.

contour, a classification of very irregular, moderately irregular, slightly irregular, or regular was assigned. The outline of the lymph node margin was also assessed for definability: A classification of indistinct, less than 50% of border distinct, or more than 50% of border distinct was assigned. In addition, the mean values of lymph node strain and surrounding neck muscle strain were measured in each region of interest, which was placed on the same image over the examined lymph node and over the surrounding neck muscles, and the muscle-to–lymph node strain ratio (ie, strain index) was calculated. Region of interest sizes ranged from 5 to 10 mm. To avoid stress decay over the examination depth, the region of interest for the muscle tissue was placed at a depth similar to the depth of the analyzed lymph node. The difference in region of interest depth never exceeded 10 mm.

Table 1

Characteristics of Examined Lymph Nodes

Imaging Examination and Characteristic	Benign Lymph Nodes ($n = 81$)	Metastatic Lymph Nodes ($n = 60$)
B-mode US		
Short-axis diameter		
<8 mm	64 (79)	32 (53)
≥8 mm	17 (21)	28 (47)
Short-to-long-axis diameter ratio		
<0.5	66 (82)	15 (25)
≥0.5	15 (18)	45 (75)
Hyperechoic hilum		
Present	44 (54)	17 (28)
Absent	37 (46)	43 (72)
Echogenicity		
Normal	74 (91)	25 (42)
Abnormal	7 (9)	35 (58)
Microcalcifications		
Present	0	2 (3)
Absent	81 (100)	58 (97)
Vascularity at power Doppler US		
Absent or hilar	80 (99)	32 (53)
Peripheral	1 (1)	28 (47)
Sonoelastography		
Visualization		
Barely or not visible	54 (67)	4 (7)
Partially or very visible	27 (33)	56 (93)
Relative brightness		
Substantially darker than surrounding muscles	4 (5)	38 (63)
Slightly darker than, brighter than, or the same as surrounding muscles	77 (95)	22 (37)
Margin regularity		
Irregular	77 (95)	39 (65)
Regular or moderately irregular	4 (5)	21 (35)
Margin definition		
<50% of Border distinct	59 (73)	31 (52)
≥50% of Border distinct	22 (27)	29 (48)
Strain index		
<1.5	79 (98)	9 (15)
≥1.5	2 (3)	51 (85)

Note.—Data are numbers of lymph nodes. Numbers in parentheses are percentages. $P < .01$ for all comparisons except that of the lymph nodes with versus those without microcalcifications ($P = .10$).

Surgery and Histologic Examination

All patients underwent lymphadenectomy and surgical removal of the primary tumor within 3 days after US. All possible measurements were taken to ensure an accurate one-to-one comparison between the lymph nodes that were imaged and those that were removed during surgery. After US examination, the location of each lymph node was mapped with respect to the surrounding anatomic structures (ie, trachea, main vessels, and sternocleidomastoid muscle) and plotted on the sketch diagram of the neck. In addition, the surgeons were assisted by a radiologist (T.H.) for correlation of the lymph node location seen on the US images with the lymph nodes seen in the lymphadenectomy specimens. After being resected, each lymph node specimen was fixed in 10% formalin, embedded in paraffin, cut into thin slices, and stained with standard hematoxylin-eosin. During histologic examination, two or three histologic slices per lymph node were examined. The final diagnosis of metastatic lymph node involvement was made by a pathologist who had 15 years of experience performing histologic cervical lymph node diagnosis. Certain additional features that can affect the elastic properties of examined lymph nodes, such as complete versus incomplete metastatic involvement and presence of necrosis and/or calcifications, were also recorded.

Statistical Analyses

Quantitative variables were compared by using the Mann-Whitney U test. Qualitative variables were compared by using the χ^2 test. The elastographic characteristics of each lymph node were registered separately and processed blindly for statistical evaluation. The unit of analysis was each lymph node rather than each patient. The value of each visual and qualitative criterion that showed the highest diagnostic accuracy in the distinction between benign and metastatic lymph nodes was selected as the cutoff value. One-way analysis of variance was performed to assess the differences in elastographic characteristics between the metastatic and benign